Journal of Molecular Structure 1200 (2020) 127115

Contents lists available at ScienceDirect

Journal of Molecular Structure

journal homepage: http://www.elsevier.com/locate/molstruc

Photocatalytic degradation of organic dyes in the presence of nanostructured titanium dioxide

H.A. Kiwaan [a], T.M. Atwee [b], E.A. Azab [a], A.A. El-Bindary [a, *]

[a] Chemistry Department, Faculty of Science, Damietta University, Damietta, 34517, Egypt
[b] Physics Department, Faculty of Science, Damietta University, Damietta, 34517, Egypt

ARTICLE INFO

Article history:
Received 20 June 2019
Received in revised form
21 September 2019
Accepted 23 September 2019
Available online 24 September 2019

Keywords:
TiO_2
Photocatalyst
Kinetics
Fluorescence

ABSTRACT

Titanium dioxide photocatalyst was synthesized through a low temperature co-precipitation process using $TiCl_4$ as a precursor for degradation of Rhodamine B (RB) Acid Red 57 (AR57) and under UV irradiation. The activities of the photocatalyst prepared at calcination temperature 400, 500 and 600 °C were investigated. The resultant TiO_2 photocatalyst was characterized by different techniques, such as XRD, SEM, EDX, N_2 adsorption and titration for the determination of the zero point charge (pH_{ZPC}). It has been found that 400 °C annealed sample of TiO_2 exhibits the highest photocatalytic dye degradation efficiency of 93.8 and 90.7% for RB and AR57, respectively within 190 min. The effect of operation parameters such as pH, catalyst dosage, initial dye concentration, as well as the influence of calcination temperatures was evaluated. Results showed that the degradation rate of dyes increased with the increased dosage of TiO_2 catalyst and decreased initial concentration of the dye. Furthermore, the kinetics and scavengers of the reactive species during the degradation were also studied. It was found that the degradation of RB and AR57 fitted the first-order kinetics and $OH^{\bullet}$ radicals were the main species. Formation of $OH^{\bullet}$ free radicals during irradiation is determined by photoluminescence studies using terephthalic acid as probe molecule.

1. Introduction

In textile industries there are large amounts of organic mixed loaded in wastewater, which causes harmful effects to the surrounding environment and human life. These wastewaters must have treated quality before reusing as possible [1,2]. Purification must be available by several different advanced techniques. Many works treated on photocatalytic degradation by using TiO_2 [3,4]. TiO_2 morphological influence in photocatalytic degradation has been studied [5,6]. The degradation methods are effective, fast, eco-friendly and easy to apply in treatment of wastewater [7–10]. Because of advanced oxidation process, the organic dyes have become an important part of industrial wastewater due to their extensive application and large-scale production. There are two families of dyes, azo dyes and thiazine dyes, which can cause rise factors of health and it is known that some azo dyes are carcinogenic. Azo dyes constituting 60–70% of all dyes formed are the largest group of dyes in textile industry and widely used due to their chemical stability and usefulness. They contain one or more azo groups (-N=N-) having aromatic rings mostly substituted by sulfonate groups. Azo dyes are resistant to biodegradation under aerobic conditions [11]. So many effective methods for decontamination of dyes in wastewater have been developed over the past decade [12,13].

Organic dyes characterize an important source of environmental contamination, since they are toxic and mostly non-biodegradable [14]. There are many different conventional treatment methods for removal these organic compounds from the industrial wastewaters, such as biodegradation, adsorption, flocculation–coagulation, electro-coagulation and conventional chemical oxidation, but they are not effective enough in achieving total removal of these organic compounds [15]. The most popular method is adsorption to remove dyes from wastewater. Various adsorbents such as activated carbons in different forms [16], clays [17,18] and carbon nanotubes [19,20] were successfully used to remove dyes from aqueous solution. On the other hand, the use of adsorption method is limited due to the high cost of adsorbents. Therefore, researches have been continuous for cheap alternative methods [17]. Except adsorption, there are many different conservative treatment

* Corresponding author.
E-mail address: abindary@yahoo.com (A.A. El-Bindary).

https://doi.org/10.1016/j.molstruc.2019.127115
0022-2860/

methods for removal these organic compounds from the industrial wastewaters, such as biodegradation, flocculation-coagulation, electro-coagulation and conventional chemical oxidation.

As known as, solar energy is a renewable resource of energy, and its efficient utilization in controlling environmental pollution by using photocatalytic materials, which reflect a one of the main targets of modern science and engineering [21]. Therefore, it is a documented metal oxide semiconductor, which could be extensively applied to diverse applications. Due to the values of its energy gap (anatase 3.2 and rutile 3.4 eV), TiO_2 can only be excited by ultraviolet light (wavelength lower than 387 nm), which occupies only 3–5% of the entire solar spectrum. Hence, the utilization of sustainable luminous energy like visible light or sunlight is limited and has no remarkable effect [22–24]. Moreover, it is also known that high recombination of activated electron-hole pair of TiO_2 is still its major drawback that causes the restriction of practical applications, in particular, solar harvesting aspect [25,26].

In the present study, we have reported the synthesis of TiO_2 photocatalyst by co-precipitation technique and then we have established the tuning of surface defects by simple thermal annealing at calcination temperatures 400, 500 and 600 °C. The sample which annealed at 400 °C showing the highest degradation efficiency of RB and AR57. SEM and XRD techniques have been used to achieve the microstructure and phase of the samples. The optimized degradation efficiency for the dye concentration has been estimated and is found to be 6 and 30 mg/L for RB and AR57, respectively. The relationship between the optical band gap (Eg) and microstructure of anatase TiO_2 has been determined and discussed. A generalized mechanism of chemical reaction of RB and AR57 dyes on photocatalysis has also been reported.

2. Materials and methods

2.1. Materials

Titanium chloride hexahydrate ($TiCl_4.6H_2O$) and oxalic acid dihydrate ($C_2H_2O_4.2H_2O$) were supplied by Sigma–Aldrich and used as received. Commercial textile dyes Rhodamine B (RB) and Acid Red 57 (AR57) were obtained from Sigma–Aldrich and was used as received. All chemical reagents were of analytical grade and used without any further purification. Samples were then conserved in the desiccator over anhydrous $CaCl_2$ for further use.

2.2. Synthesis of TiO_2 photocatalyst

TiO_2 was synthesized through a low temperature co-precipitation process using deionized water as a solvent. An aqueous ammonia (10%, 100 mL) was added drop wisely to titanium chloride hexahydrate (0.5 mol, 54.9 mL) dissolved in deionized water until reached pH = 9.5. The resulting material was separated by filtration, washed for several times with 2% NH_4Cl solution and then with hot distilled water till free from chloride ion and dried at 110 °C for 24 h. The white precipitate of $Ti(OH)_4$ was formed. Finally, TiO_2 was obtained by thermal treatment at different calcination temperatures of 400, 500 and 600 °C for 5 h. Moreover, the dried TiO_2 samples were sieved with a 200 μm mesh in order to obtain small uniform particles.

2.3. Catalyst characterization

FTIR analysis was carried out using a JASCO-FT/IR-4100 spectrometer (Jasco, Easton, MD, USA): the finely grinded sample of TiO_2 was included into KBr discs prior to analysis in the wavenumber range 400–4000 cm^{-1}. The surface morphology of TiO_2 photocatalyst was examined using scanning electron microscope (SEM) investigation at accelerating voltages of 20 kV (JEOL-JSM-6510 LV) using gold coating examination. The elemental distribution of TiO_2 was analyzed using the energy-dispersive X-ray spectroscopy (EDX) and taken on a Leo1430VP microscope with operating voltage 5 kV. Structural deviations of the as-prepared samples was investigated by X-ray diffraction (XRD) system using a Shimadzu XRD-6000 diffract meter (Shimadzu Corporation, Tokyo, Japan) equipped with Cu Kα radiation (λ = 1.54 Å). The 2è range was varied between 5 and 80° at a scanning rate of 0.02°. The crystal system, space group and lattice parameters values were measured and optimized using CRYSFIRE and CHEKCELL computer databases [27]. UV–visible spectrophotometer (PerkinElmer AA800 spectrophotometer Model AAS) was working for absorbance measurements of samples using 1.0 cm quartz cell. Fluorescence Spectrometer (LUMINA, Thermo Scientific) was used for fluorescence measurements of samples using 1.0 cm quartz cell. The adsorption/desorption isotherm of N_2 on TiO_2 at $P/P_o = 6.58 \times 10^{-5}$ torr and 77 K was performed with a Quantachrome Touch Win Instruments version 1.11. HANNA instrument pH meter (model 211) was used for pH modification. HANNA instrument wastewater behavior photometer (model HI 83214) was used for the measurement of chemical oxygen demand (COD).

2.4. Determination of point of zero charge

The point of zero charge (pH_{PZC}) was resolute by solid addition method [28]. A series of 50 mL (0.1 M) KNO_3 solutions were prepared and their pH values (pH_0) were adjusted in the range of 1.0–10.0 by adding of 0.1 M HCl and 0.1 M NaOH. To every solution, 0.1 g of TiO_2 was added and the suspensions were concerned in an orbital shaker at 200 rpm. The final pH values of the supernatant were determined (pH_f) after 48 h. The difference between initial (pH_0) and final (pH_f) values ($\Delta pH = pH_0 - pH_f$) (Y-axis) was plotted against the initial pH_0 (X-axis). The intersection of resulting curve yielded the pH_{PZC} where ΔpH = zero.

2.5. Photocatalytic dye degradation experiments

The photocatalytic activity of prepared TiO_2 photocatalyst was evaluated by monitoring the photodegradation of Rhodamine B and Acid Red 57 in aqueous solution using UV lamp under atmospheric condition. The specifications of the UV lamp used in the experiment are E_{photon} (eV) 4.43–12.4 with λ_{max} (nm) 280-100 [29]. A 150 mL beaker (5 cm inside diameter) was utilized as a reactor for performing dye degradation experiments. The distance from the lamp to the top solution surface was fixed to 10 cm. The working volume of the reactor was 100 mL, having dye solution and photocatalyst suspension. The photocatalyst samples of TiO_2 (2.5 g/L) were added into a 100 mL of RB (6 mg/L) and AR57 (30 mg/L) dye solution maintained at the pH of 7. Effective stirring of dye solution and photocatalyst is essential in order to keep the uniform dispersion of the photocatalyst with reduced agglomeration. Before illumination, the solution was stirred continuously at 600 rpm by magnetic stirrer in dark for 30 min for the powder photocatalyst to adsorb the dye in the solution and reach adsorption desorption equilibrium. Thus, the effect of surface adsorption in the removal of RB and AR57 is eliminated.

The influence of the pH of the initial solution was evaluated at pHs from 2 to 10 (adjusted using HCl (0.1 M) and NaOH (0.1 M)). Catalyst dosage was varied from 0.1 to 0.5 g/L, keeping RB and AR57 dye concentration at 6 and 30 mg/L, respectively. The influence of dye concentration using 2.5 g/L of TiO_2 photocatalyst was also evaluated by changing its concentration from 4 to 9 and from 10 to 50 mg/L for RB and AR57 dye, respectively. Each sample was taken

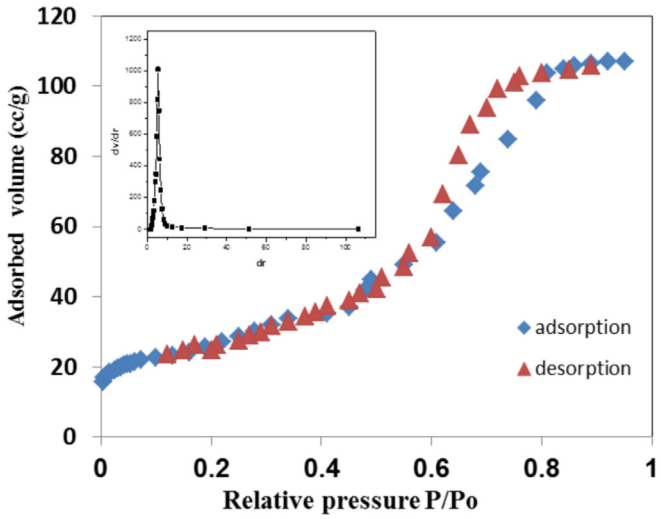

Fig. 1. N_2 adsorption/desorption isotherm curve of TiO_2 at 400 °C and at 77 K.

out at a given time interval and immediately centrifuged at 20,000 rpm for 5 min to remove any suspended solid catalyst particles for analysis. In order to maintain the temperature inside the enclosure, an exhaust fan is required. Finally, the absorbance of RB and AR57 in the sup ernatant liquid was recorded by a UV−visible spectrophotometer, at the maximal absorption wavelength of RB ($\lambda_{max} = 545$ nm) and AR57 ($\lambda_{max} = 512$ nm).

The degradation rate (D) of the dye was calculated using Eq. (1):

$$D\,\% = (A_0 - A_t)/A_0 \times 100 \quad (1)$$

where A_0 denotes the initial absorbance of RB and AR57 solution (blank), and A_t its absorbance after t minutes of irradiation/reaction. According to the Beer−Lambert's law A_0 and A_t are proportional to C_0 and C_t, where C_0 and C_t are the concentration of blank and sample at (t) time.

To confirm the photodegradation results, chemical oxygen demand (COD) of samples before and after photodegradation experiments was measured at regular time intervals [29]. The photodegradation of pollutants follows the pseudo first-order kinetics according to the Langmuir−Hinshelwood model [30], so the photodecolorization rate of each dye was studied using Eq. (2):

$$\ln (C_0/C_t) = \ln (A_0/A_t) = kt \quad (2)$$

The photo degradation rate constant (k, min^{-1}) was calculated from the slope of the straight-line segment of the plot of $\ln (C_0/C_t)$ *vs.* t as a function of the used experimental parameters.

The optical properties of the photo catalysts were studied by UV−visible absorption spectroscopy at room temperature. The powder samples were dispersed in paraffin oil by sonication and their optical properties were studied in the wavelength range 200−800 nm, with paraffin oil as the reference medium [31].

The photocatalytic stability of TiO_2 (at 400 °C) was also evaluated for three cycle times under same conditions. In addition, the active species such as hydroxyl radical ($OH^{\bullet}$), electron (e^-), hole (h^+) and super oxide ($O_2^{\bullet -}$) were also performed with different free radical scavengers (iso-propanol, silver nitrate, potassium iodide and *p*-benzoquinone) under UV light irradiation at the similar conditions.

3. Results and discussion

3.1. Brunauer-Emmett-Teller (BET) specific surface area

The Brunauer-Emmett-Teller (BET) [32] specific surface area and Barrett-Joyner-Halenda (BJH) pore size of TiO_2 have been investigated using N_2 adsorption/desorption measurements at 77 K (Fig. 1). The N_2 adsorption-desorption isotherm of TiO_2 nanoparticles is classified as type II that referred to non-porous solid at $P/P_o = 0.9868$. The isotherm is completely reversible without showing any hysteresis loop illuminating the absence of any pore type that permit capillary condensation process. The specific surface area of TiO_2 at different calcination temperature (Table 1) was calculated by BET equation in its normal range of applicability and adopting a value of 16.2 Å for the cross-section area of N_2 molecule. Also, the total pore volume taken at a saturation pressure and the pore radius calculated by BJH pore size distribution curve were calculated (Table 1) [33,34]. In our case, the photocatalytic efficiency is higher for sample at calcination temperature 400 °C, having smaller crystallite size than the others, higher specific surface area (156.036 m^2/g). Hence this catalyst was used in the next experiments.

3.2. X-ray diffraction

The XRD patterns of the as arranged TiO_2 nanostructures at

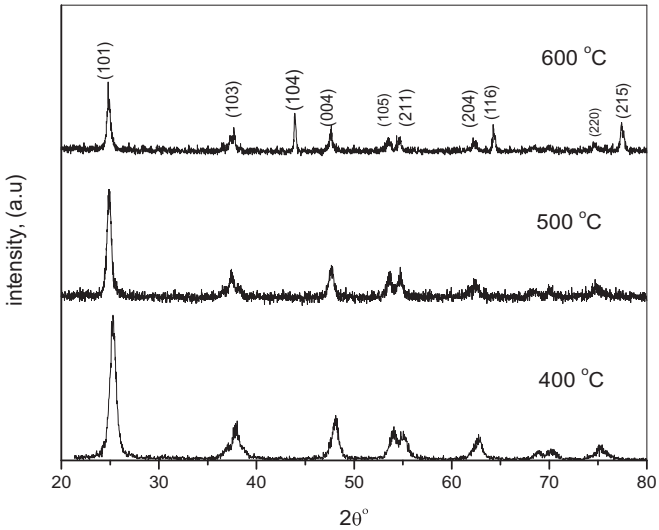

Fig. 2. X-ray diffraction patterns of TiO_2 nanostructures at different annealing temperatures 400, 500 and 600 °C.

Table 1
Specific surface area, pore volume and average pore size of TiO_2 nanostructure calcined at different temperatures.

Temperature °C	Specific surface area (m^2/g)	Pore volume (cm^3/g)	Average pore size (nm)	R^2
400	156.036	0.1890	3.485	0.9981
500	87.121	0.4582	5.058	0.9287
600	33.800	0.7054	9.681	0.9881

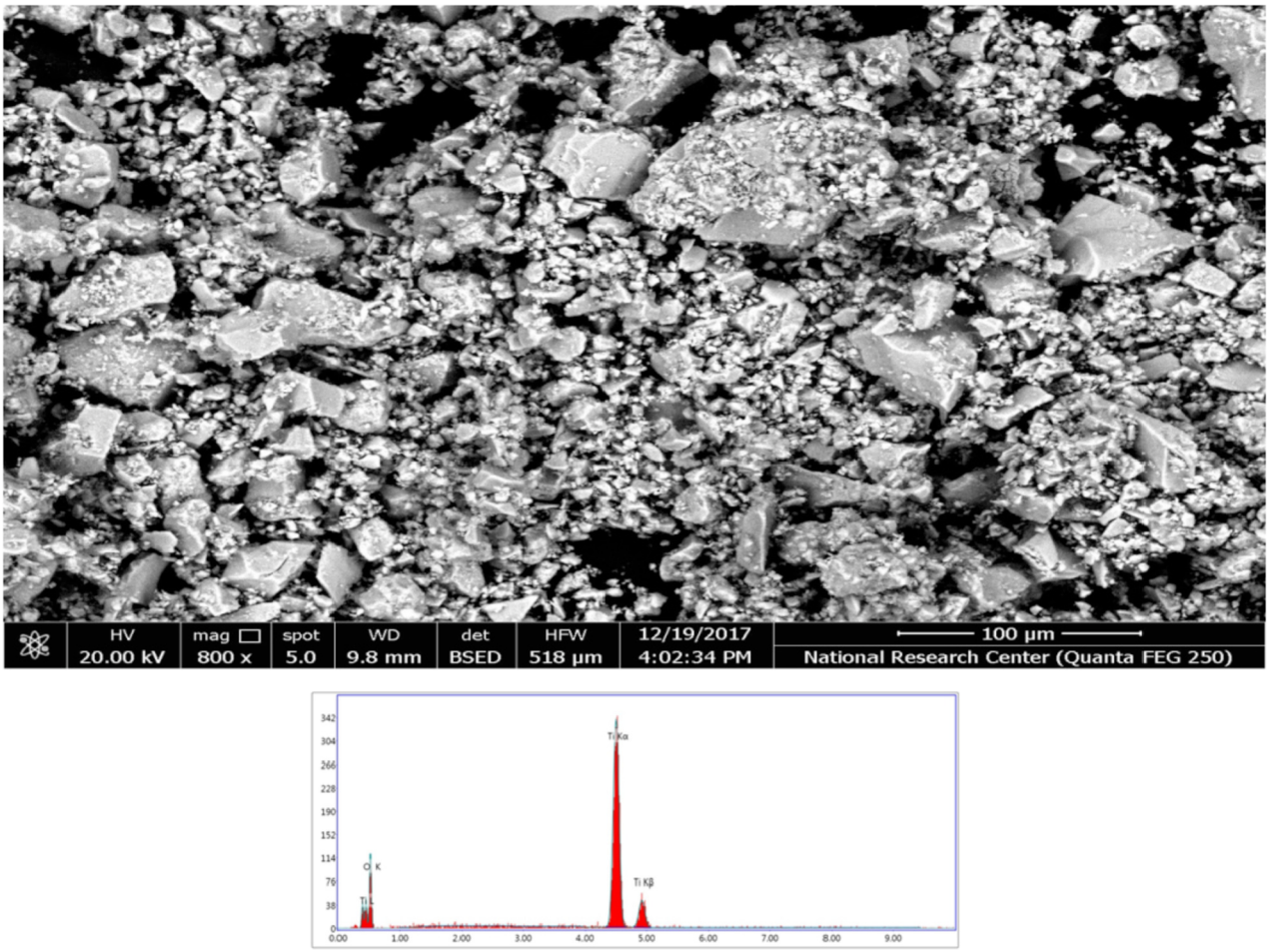

Fig. 3. a. SEM image of TiO_2 nanostructures at calcination temperature 400 °C. b. Energy Dispersive X-ray (EDX) spectrum of TiO_2 at 400 °C.

different thermal treatment temperatures 400, 500 and 600 °C are shown in Fig. 2. The observed diffraction peaks communicate to well crystallized TiO_2 indicates the formation of titania anatase structure (JCPDS No. 21−1272) with lattice constant a = b = 3.786 Å and c = 9.507 Å [35]. It can be seen that the XRD patterns of TiO_2 samples are similar at different annealing temperatures (Fig. 2). No additional peaks due to impurities were detected indicating the high purity of the as-prepared TiO_2, and the peaks at 2θ = 25.34, 37.82, 38.10, 48.08, 53.94, 55.10, 62.78, 68.80, 70.59 and 75.2° can be attributed to (101), (103), (004), (200), (105), (211), (204), (116), (220) and (215) planes of TiO_2, respectively [36]. The crystallite size (D, Å) of the TiO_2 nanoparticles was calculated by using the Scherrer's formula (Eq. (3)) [37],

$$D = K\lambda\beta \cos\theta_B \quad (3)$$

where, λ is the X-ray wavelength (1.54 Å), β is the angular width of the peak at half of its maximum intensity (full-width at half-maximum) corrected for the instrumental broadening, θ_B is the maximum of the Bragg diffraction peak and *K* is Scherrer's constant (0.9 Å).

The average crystallite size of TiO_2 was calculated from the main peak (2θ = 25.34°) of XRD patterns, which corresponds to the plane (101). The estimated crystallite size was 12.5, 17.12 and 18.6 nm at annealing temperatures 400, 500 and 600 °C, respectively. These results can be explained on the basis of increased extent of agglomeration of the TiO_2 particles with increasing annealing temperature which also result in the decrease of the surface area [38,39].

3.3. SEM and EDX analysis

The surface morphology and surface area are very effective parameters in photocatalytic activity of TiO_2 nanoparticles. TiO_2 nanoparticles due to the high surface energy tend to be aggregated. This agglomeration deteriorates the photocatalytic activity through the reduction of effective surface area of TiO_2 nanoparticles. TiO_2 nanoparticles at calcination temperature 400 °C were investigated through SEM analysis (Fig. 3a). This SEM image show closely packed nearly spherical and randomly oriented nanoparticles [40].

Energy dispersive X-ray investigation is established on the principle of unique atomic structure provides unique set of peaks on its X-ray spectrum for each element. The elemental composition of TiO_2 nanostructure was determined by EDX analysis coupled with SEM. Peaks assigned to Ti and O were set up, but no impurity peaks were detected, which further long-established that the synthesized TiO_2 is pure and consists of only Ti and O (Fig. 3b). Ti signal at 5.00, 4.50 and 0.40 keV, and oxygen peak at 0.58 keV and was detected.

3.4. Optical band gap energy (E_g)

The quantity of the energy band gap of TiO_2 nanostructures has been determined by studying of the optical properties of these

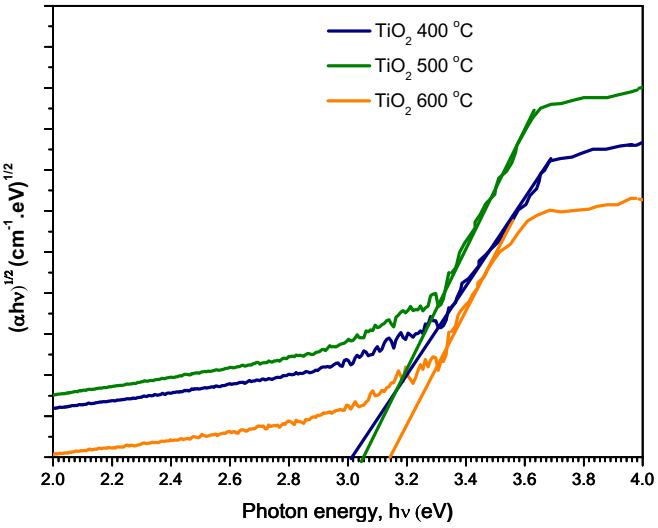

Fig. 4. The optical band gap energy determination of TiO_2 at annealing temperatures 400, 500 and 600 °C using Tauc's model for n = 2.

particles using UV–visible spectroscopy. The band gap energy of semiconductors was determined using Tauc's formula [41] which shows the relationship among absorption coefficient as follows (Eq. (4)):

$$(\alpha h\upsilon)^{1/n} = A\left(h\upsilon - E_g\right) \quad (4)$$

where α is the absorption coefficient, h is Planck's constant and υ is the frequency of vibration (υ = c/λ, where λ is the wavelength and c is the light speed) [42]. Exponent n depends on the type of transition and it may have values 1/2, 2, 3/2 and 3 corresponding to the allowed direct, allowed indirect, forbidden direct and forbidden indirect transitions, respectively [43]. ***A*** is a constant depending on the transition probability and generally called band tailing parameter. In the case of amorphous, homogeneous semiconductors n is 2 independently of the type of transition [44]. In case of TiO_2, n = 2 is usually considered. Thus, the band gap energy was obtained graphically from $(\alpha h\upsilon)^{½}$ *vs.* hυ (Fig. 4), extrapolating the linear part on the abscissa according to Eq. (4). The band gap energy was found to be 3.00, 3.05 and 3.15 eV for TiO_2 at annealing temperature 400, 500 and 600 °C, respectively. It was observed that energy band gap increases with increase in annealing temperature. In general, the band gab value depends on crystallite size and structural parameter [34,45].

3.5. FTIR analysis

Infrared studies were carried out in order to establish the purity and nature of the metal nanoparticles. Metal oxides generally give absorption bands in fingerprint region i.e. below 1000 cm^{-1} arising from inter-atomic vibrations. The peaks at 464 and 836 cm^{-1} ascribed to the Ti–O stretching vibration mode [46]. Also, the catalyst surfaces were adsorptive to atmospheric CO_2 as ascribed from the less intense peaks at 1408 and 2922 cm^{-1} [47]. The peaks around 3440 cm^{-1} are the stretching vibration of O–H in adsorbed water and those at 1633 cm^{-1} are the bending vibration of Ti–OH [48].

3.6. Determination of point of zero charge (pH_{PZC})

pH was one of the most important parameters for the degradation of RB and AR57, as it resolute which ionic species were nearby in the adsorbate solution and the surface charge of the sorbent. Surface charge of the TiO_2 was determined by the PZC, which is defined as the pH (pH_{PZC}) at which the positive charges on the surface equal the negative charges [49]. The pH_{PZC} of TiO_2 was found to be 7.18. This shows that below this pH, the TiO_2 acquires a positive charge owing to protonation of functional groups and above this pH, negative charge exists on the surface of TiO_2.

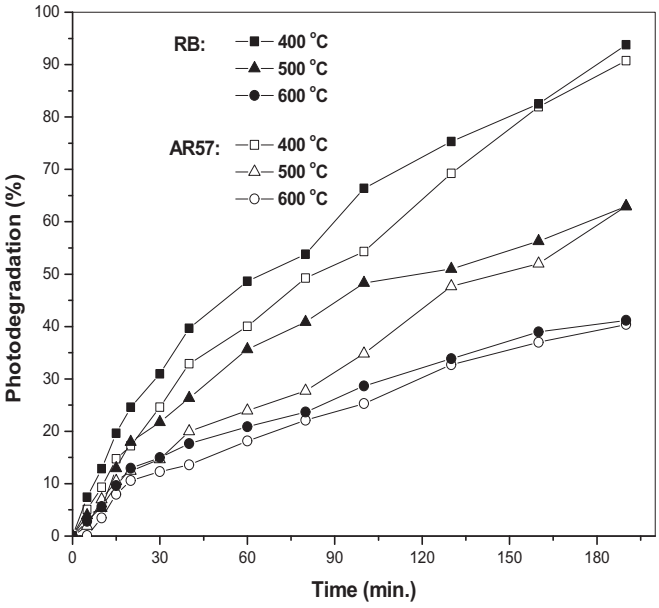

Fig. 5. Effect of calcination temperature on the properties of TiO_2 (6 mg/L initial dye concentration of RB, 30 mg/L initial dye concentration of AR57, 2.5 g/L TiO_2, and pH = 7).

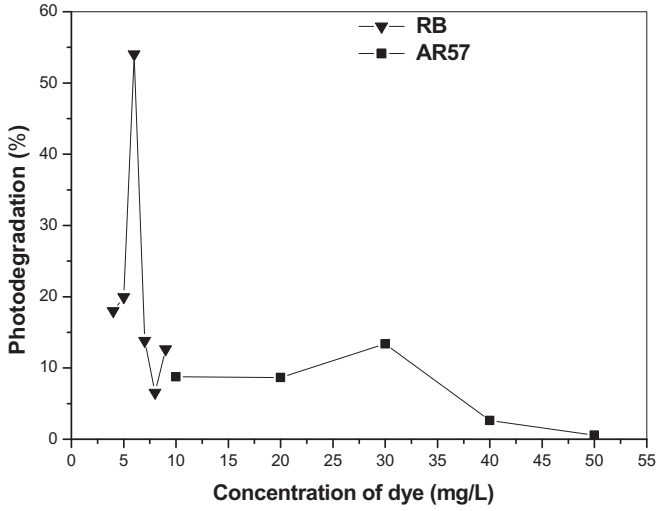

Fig. 6. Effect of initial dye concentration on the photodegradation activity of TiO_2 at 400 °C (30 min of irradiation time 2.5 g/L TiO_2, and pH = 7).

3.7. Effect of operating parameters on the photocatalytic degradation of RB and AR57

3.7.1. Effect of calcination temperature

The activities of the prepared photocatalyst (TiO_2) at different calcination temperatures 400, 500 and 600 °C were investigated.

The degradation rate of RB and AR57 over TiO_2 improved with decrease of the calcination temperature. At the calcination temperature of 400 °C, the degradation rate reached 93.8 and 90.7% for RB and AR57, respectively (Fig. 5). The degradation efficiency of the TiO_2 samples followed the order 400 > 500 > 600 °C after UV irradiation for 190 min, which may be associated to the particle size of the photocatalyst (Table 1). When the calcination temperature of TiO_2 increased from 400 °C to 600 °C the photocatalytic reaction rate tends to decrease at higher calcination temperature (rutile structure). The photocatalytic activity of TiO_2 generally increased with increasing crystallization and decreased with decreasing specific surface area (Table 1). Higher calcination temperature could promote the crystallization of TiO_2 and efficiently remove the bulk defects sites for the recombination of the photo-induced electron−hole pairs [31].

3.7.2. Effect of initial dye concentration

The effect of initial dye concentration on its degradation has been studied with varying concentration of dye from 4 to 9 mg/L for RB and from 10 to 50 mg/L for AR57, keeping the TiO_2 catalyst concentration set at 2.5 g/L (Fig. 6). It is found that the degradation efficiency of TiO_2 sample has been increased initially for dye concentration up to 6 mg/L for RB and up to 30 mg/L for AR57 and then decreased [50]. Therefore, the removal efficiency of dye could be improved by the lower initial concentration of the dye [51]. This may be explained that more and more dye molecules were adsorbed on the photocatalyst surface, when initial dye concentration was increased. Since many active sites were full by the dye molecules, the adsorption of O_2 and OH^- on the photocatalyst was decreased, which leads to reduced regeneration of radicals [52]. Moreover, the photons were blocked before realization the photocatalyst surface; hence, the adsorption of photons was decreased by the photocatalyst.

3.7.3. Effect of TiO_2 dosage

Sufficient dosage of the catalyst increases the generation rate of electron/hole pairs and thus the formation of $OH^\bullet$ radicals for attractive photodegradation efficiency. Hence the catalyst dosage effect on the degradation efficiency of the process was studied in the range of 0.1−0.5 g/L keeping RB and AR57 dye concentration at 6 and 30 mg/L, respectively (Fig. 7). As shown, the photocatalyst amount of 2.5 g/L showed the best efficiency toward the decolorization of RB and AR57 and then a sharp decrease was happened in the decolorization efficiency. By increasing the photocatalyst amount, more and more active sites were found on the photocatalyst surface, which leads to enhance of formation of hydroxyl radicals [53]. Negative effect was observed by additional increase of the photocatalyst amount; because aggregation of catalyst particles shows screening affect which can avoid getting to photons to inner catalyst surface [54]. However, an excess dosage of the catalyst decreases the light penetration via protecting effect of the suspended particles and hence reduces photodegradation rate.

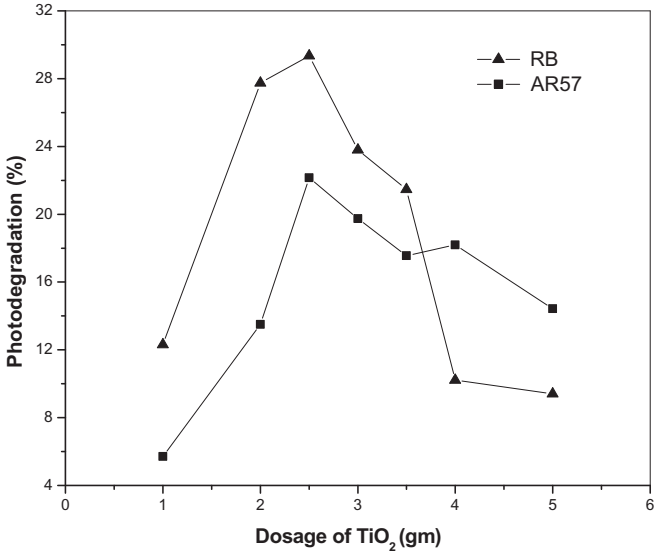

Fig. 7. Effect of TiO_2 concentration prepared at 400 °C on the photodegradation activity of RB (6 mg/L) and AR57 (30 mg/L) at 20 min irradiation time and pH = 7.

3.7.4. Effect of pH

pH is a significant operational parameter determining the efficiency of the photocatalytic removal of different pollutants in wastewaters [55]. The effect of varying pH from 2 to 10 in the initial dye solution is shown in Fig. 8, for an initial concentration of RB (6 mg/L) and AR57 (30 mg/L), over TiO_2 (2.5 g/L), and under UV irradiation [56]. Adsorption and thus dye degradation appear to be chosen at pH around the zero-point charge pH (pHzpc), i.e., 7.18 for the TiO_2. At a pH higher than 7.18 the surface of TiO_2 photocatalyst is negatively charged, whereas at pH lower than 7.18 it converts posatively charged. Since RB and AR57 is anionic type dye, a pH lower than that corresponding to the zero-point charge favors the adsorption of RB and AR57 molecule on the catalyst surface which results in improved degradation of RB and AR57 under neutral and acidic conditions.

Furthermore, in acidic condition, the molecular structure of the dye might change into the quinoid structure, which is unstable and might be easily destroyed. Though, a further increase in pH principals to an increase coulombic repulsion between the negative charged TiO_2 surface and the OH^- species involved in the photocatalytic oxidation mechanism [57], leading to decreased degradation efficiency.

3.8. Estimation of chemical oxygen demand (COD)

Organic strength of wastewater can be estimated in terms of the total quantity of oxygen required for the oxidation of organic matter to CO_2 and H_2O [58]. The COD value of the dye solution before and after the treatment was estimated. Chemical oxygen demand was measured after exposure the sample to UV irradiations at times 0, 30, 60 min to check the photodecolorization of RB and AR57 dyes and found to be 227, 135, 80 and 145, 110, 63 ppm, respectively. The observed decrease in the COD values of the preserved dye solution with increasing time indicating the complete mineralization of dye into non-toxic species.

3.9. Degradation kinetics

Rhodamine B (RB) and Acid Red 57 (AR57) were utilized as model dyes to evaluate the photocatalytic activity of the prepared TiO_2 sample under simulated UV radiation. The absorbance curve of RB and AR57 solutions after 190 min of irradiation is shown in Fig. 9 using as prepared and calcined TiO_2 at 400 °C as photocatalyst. The kinetics of RB and AR57 photodegradation on the photocatalyst surface can be described by the first-order reaction as shown in Eq. (2). Fig. 9 designates the linear relationship of ln (C_0/C_t) *vs.* irradiation time (t) for the solution of RB and AR57. Rate constants were determined for analyzed photocatalyst from the slope of linear fitting line as shown in Fig. 9. As it can be seen, a good correlation to the first order reaction kinetics ($R^2 = 0.989$) was found. In our case, RB degraded faster as compared to AR57 due to the lower bond dissociation energy of RB. Bond dissociation energy theory states

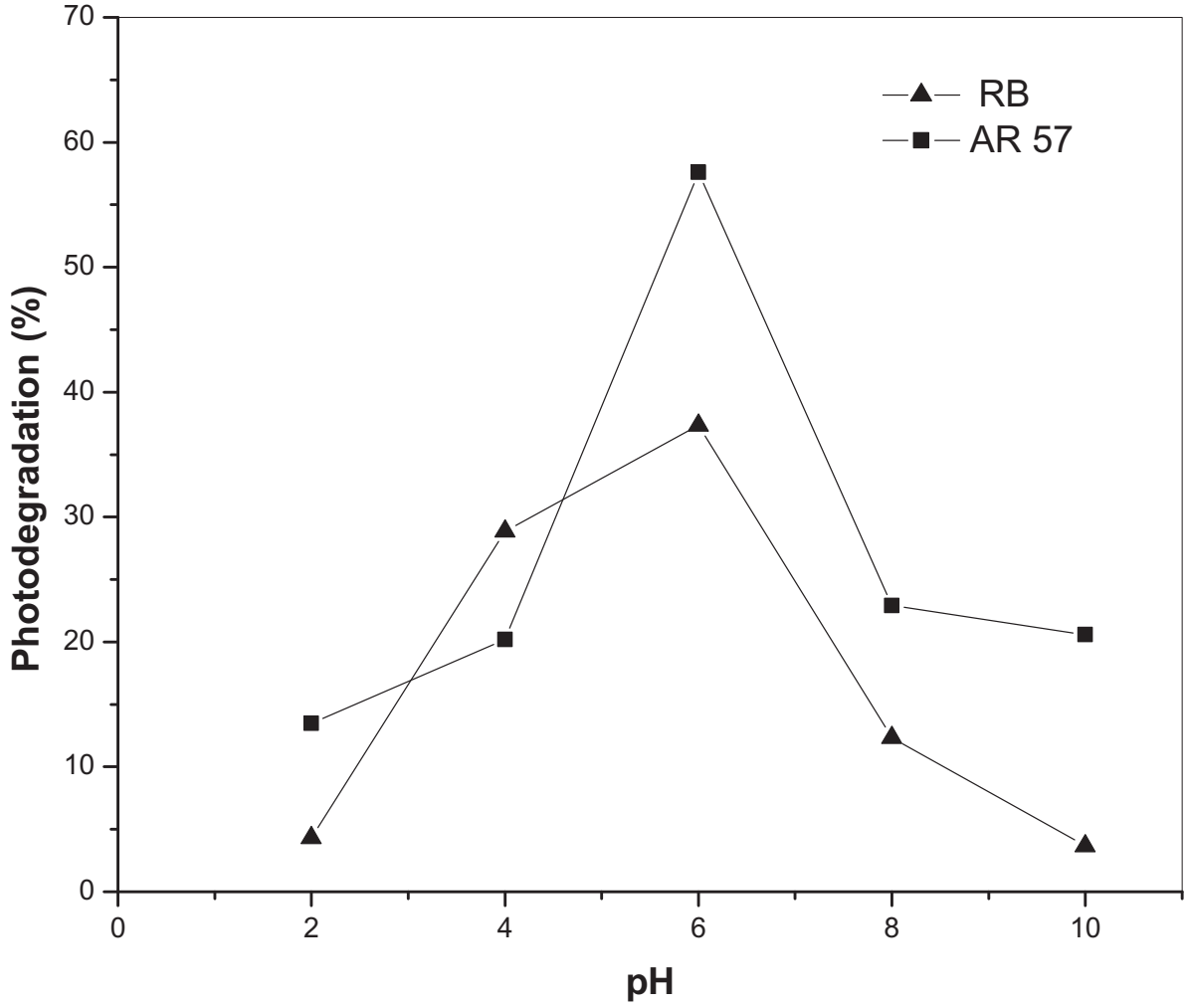

Fig. 8. Effect of pH on the properties of TiO_2 at 400 °C (20 min irradiation time, 6 mg/L for RB and 30 mg/L for AR57 initial dye concentration, 2.5 g/L TiO_2 and pH 7).

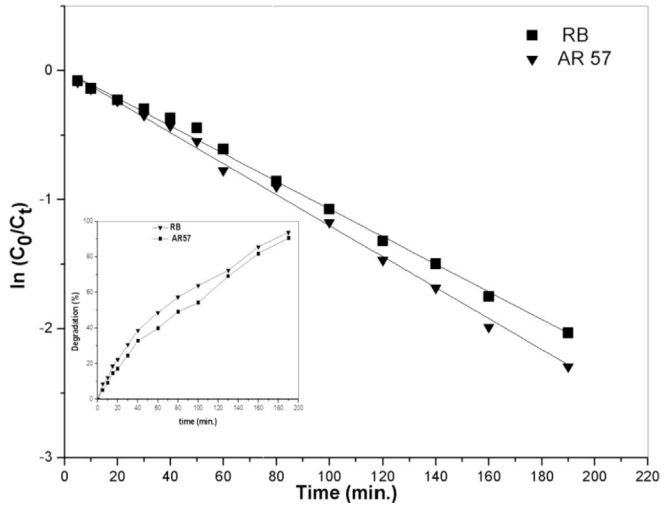

Fig. 9. Photocatalytic degradation efficiency of RB and AR57 using TiO_2 under simulated UV irradiation.

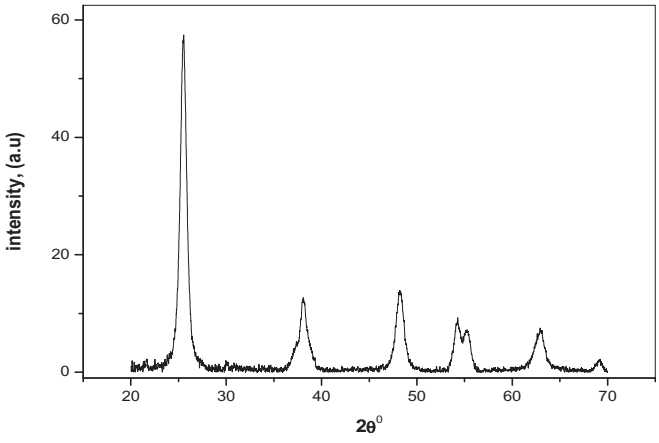

Fig. 10. X-ray diffraction pattern of TiO_2 nanostructures at 400 °C after three times recycling.

that chemical bonds with lower bond dissociation energy are easier to break and suitably, form new bonds [59,60]. The rate constant of RB and AR57 was found to be 0.120 and 0.107 min^{-1}, respectively.

3.10. Stability of photocatalyst TiO_2

Recycling experiments of TiO_2 for the photocatalytic

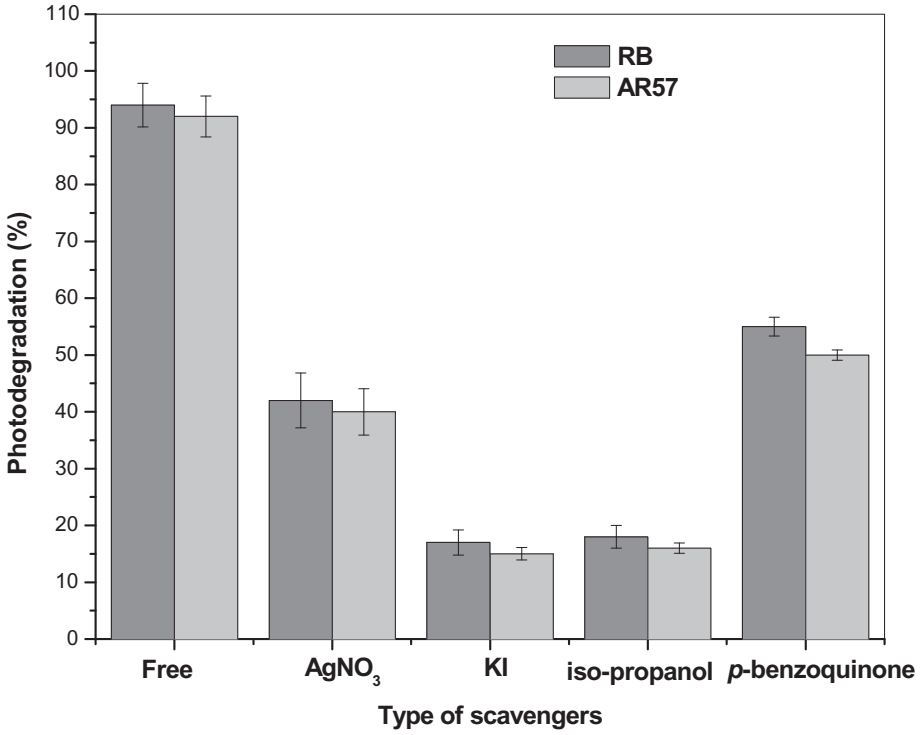

Fig. 11. Photodegradation ratio of RB and AR57 over TiO_2 at 400 °C in the absence and presence of various scavengers (*p*-benzoquinone, KI, iso-propanol and silver nitrate) under UV irradiation at the optimum conditions.

degradation of RB and AR57 under UV irradiation were carried out to investigate its stability. The photocatalyst was collected after each cycle by centrifugation, then washed with distilled water and ethanol and dehydrated in an oven at 100 °C. The sample was then reused for subsequent degradation. As can be seen, the efficiency of the degradation of RB and AR57 reduced from 93.8 to 87 and 90.7 to 85 after three cycles, respectively. The photocatalytic activity of TiO_2 only minimally decreases, due to the unavoidable loss of photocatalysts during the cycle processes. Consequently, the TiO_2 photocatalyst remains high photocatalytic activity and stability under UV irradiation for a long time (Fig. 10).

3.11. Mechanism of photodegradation

The photocatalytic reaction generally contains photoexcitation, charge separation, migration and surface oxidation–reduction reactions [61]. Through the photodegradation of dyes over TiO_2, the e^-, h^+, $OH^\bullet$ and $O_2^{\bullet-}$ are reduced by adding $AgNO_3$ (e^- scavenger), potassium iodide (h^+ scavenger), iso-propanol ($OH^\bullet$ scavenger) and *p*-benzoquinone ($O_2^{\bullet-}$ scavenger) into the reaction solution, respectively [62]. Fig. 11 shows the degradation rate in the presence and absence of the scavengers at the same conditions [63]. Hence, the active species responsible for photocatalytic degradation of RB and AR57 is the holes in valence band (h^+) electron conduction band (e^-) and hydroxyl radicals ($OH^\bullet$). The efficiency of photocatalysts for degradation of the two dyes is mainly influenced by the concentration of the generated $OH^\bullet$ radicals.

Once TiO_2 is exposed to the photons (hυ) with the energy equivalent or higher than the band gap energy (E_g), electrons are excited from the valence band (VB) to conduction band (CB) leaving holes behind in VB and thus form electron–hole pairs. Firstly, the diffusion of organic pollutants takes place from the polluted solution to the photocatalyst surface. Then, the effective adsorption of the redox reaction and desorption of the product to the outer surface of the photocatalyst. Then, the removal or separation of the lessor non-toxic product to the treated solution is executed. The fundamental mechanism of photocatalytic degradation of RB and AR57 can be illustrated:

$$TiO_2 + h\upsilon \rightarrow TiO_2\left(h^+_{(VB)}\right) + TiO_2\left(e^-_{(CB)}\right) \quad (5)$$

The electrons generated through irradiation could be readily surrounded by O_2 absorbed on the photocatalyst surface or the dissolved O_2 [64] to give superoxide radicals ($O_2^{\bullet-}$):

$$e^-_{(CB)} + O_2 \rightarrow O_2^{\bullet-} \quad (6)$$

Consequently, $O_2^{\bullet-}$ could react with H_2O to yield hydroperoxy radical ($HO_2^\bullet$) and hydroxyl radical ($OH^\bullet$), which are strong oxidizing agents to decompose the organic molecule:

$$O_2^{\bullet-} + H_2O \rightarrow HO_2^\bullet + OH^\bullet \quad (7)$$

Simultaneously, the photoinduced holes could be surrounded by surface hydroxyl groups (or H_2O) on the photocatalyst surface to give hydroxyl radicals ($OH^\bullet$):

$$OH^- + h^+_{(VB)} \rightarrow OH^\bullet_{ad}$$

$$H_2O \leftrightarrow \left(H^+ + OH^-\right) + h^+_{(VB)} \rightarrow OH^\bullet + H^+ \quad (8)$$

Finally, the organic molecules (RB or AR57) will be oxidized to yield carbon dioxide and water as follows:

$$OH^\bullet + \text{RB or AR57} + O2 \rightarrow \text{products}\ (CO_2 \text{ and } H_2O) \quad (9)$$

Meanwhile, recombination of positive hole and electron could happen which could reduce the photocatalytic activity of prepared nanocatalyst (TiO_2):

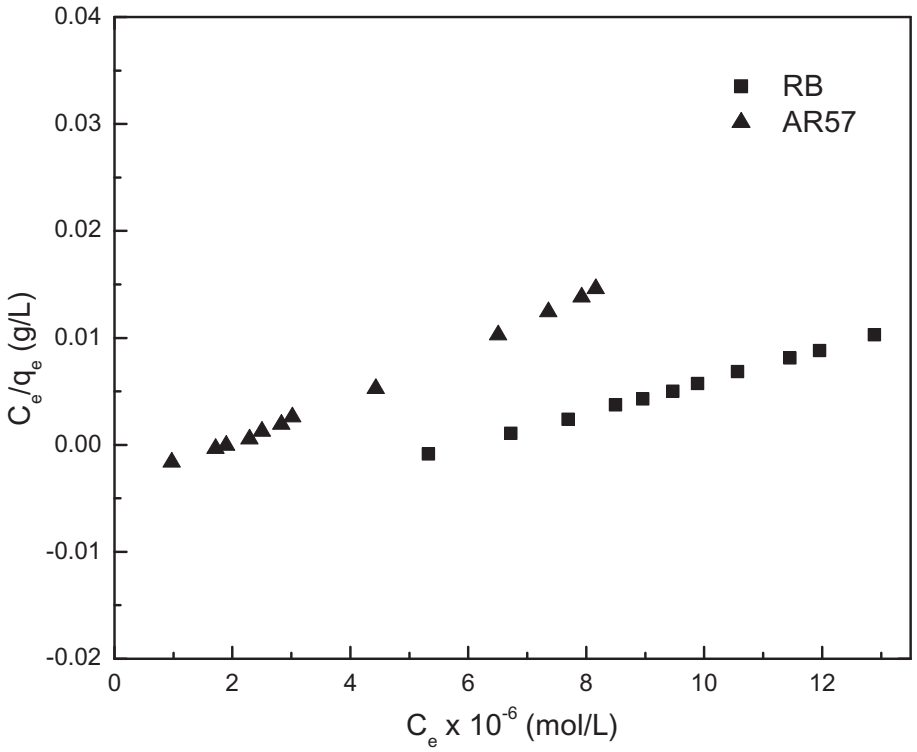

Fig. 12. Langmuir plots for adsorption of RB and AR57 onto TiO_2 at 400 °C.

$$TiO_2(h^+_{(VB)}) + TiO_2\ (e^-_{(CB)}) \rightarrow TiO_2 \quad (10)$$

Photoluminescence studies using terephtalic acid (TPA) as a probe molecule were used to determine the formation of $OH^\bullet$ free radicals. TPA is recognized to react with $OH^\bullet$ free radicals to yield 2-hydroxyterphthalic acid displays a characteristic luminescence peak at 420 nm [65]. The intense luminescence peak at 420 nm for sample containing TiO_2+TPA after irradiation for 30, 60, 90, 120 and 180 min showed clearly the presence of $OH^\bullet$ free radicals during irradiation.

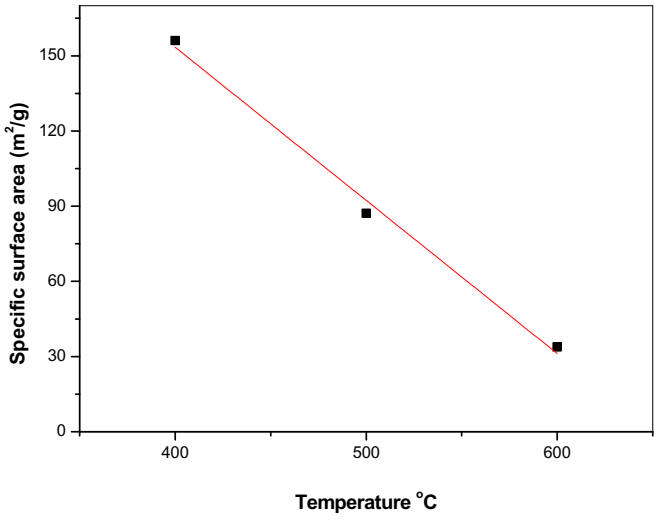

Fig. 13. Correlation curve between specific surface area of TiO_2 at 400, 500 and 600 °C and photodegradation efficiency of RB and AR57.

3.12. Adsorption isotherms

Adsorption on a uniform surface with equivalent adsorption capacity is well described by the Langmuir isotherm, which suggests monolayer adsorption [66]. Furthermore suggests no additional adsorption of dye molecules shield the active sites on the adsorbent. The Langmuir adsorption isotherm was used (Eq. (11)):

$$C_e/q_e = 1/(q_{max}K_L) + C_e/q_{max} \quad (11)$$

where C_e is the equilibrium dye concentration in solution (mol/L), q_e is the equilibrium dye concentration in the adsorbent (mol/g), q_{max} is the monolayer capacity of the adsorbent (mol/g) and K_L is the Langmuir adsorption constant (L/mol). Then, a plot of C_e/q_e *vs.* C_e gives a straight line of slope $1/q_{max}$ and the intercept $1/(q_{max}K_L)$ (Fig. 12). The Langmuir equation is appropriate to homogeneous sorption, where the sorption of each sorbate molecule onto the surface is equal to sorption activation energy [17]. The maximum monolayer adsorption capacity (q_{max}) was found to be 6.75×10^{-4} and 4.38×10^{-4} mol/g for RB and AR57, respectively. Langmuir adsorption constant (K_L) were found to be and 1.66×10^5 and 5.21×10^5 L/mol for RB and AR57, respectively. High correlation coefficient (R^2) values (0.9992 and 0.9976 for RB and AR57, respectively) of the straight lines obtained confirm the validity of Langmuir adsorption isotherm [67].

3.13. Correlation analysis

It is important to study the relationship between the physical and chemical properties of the photocatalyst and its degradation properties. The degradation efficiency of TiO_2 photocatalyst at 400, 500 and 600 °C was found to be 93.8, 67.3 and 36.9% and 90.7, 62.9.67 and 40.3% for the RB and AR57, respectively after 190 min. UV irradiation. Fig. 13 shows that the relation between the specific

surface area of the photocatalyst at (400, 500 and 600 °C) and its degradation efficiency for the dyes. The specific surface area of TiO_2 which calculated from BET measurements at 400, 500 and 600 °C was found to be 156.036, 87.21 and 33.800 m^2/g, respectively. As the calcination temperature increases, the specific surface area decreases, the average pore size increases, and the photocatalyst will result in a low degradation rate of dyes. Therefore, the best photocatalytic degradation of RB and AR57 was observed over TiO_2 at 400 °C.

4. Conclusions

In this work the photocatalytic activity of TiO_2 photocatalyst was studied for the treatment of aqueous solutions containing RB and AR57 under UV light irradiation. TiO_2 sample was synthesized by co-precipitation method and calcined at different temperatures and they were characterized by different spectroscopic techniques. Based on the XRD and SEM measurements, the TiO_2 was present as hexagonal wurtzite phase and the size of TiO_2 was 12.5, 17.12 and 18.6 nm at annealing temperatures 400, 500 and 600 °C, respectively. In fact, the highest photocatalytic removal of RB and AR57 from aqueous solution was achieved by using TiO_2 as photocatalyst, confirmed also by the evaluation of the kinetic constant for RB and AR57 degradation. The effect of operation parameters such as pH, catalyst dosage and initial dye concentration was estimated. It was found that the degradation of RB and AR57 fitted the first-order kinetics and $OH^•$ radicals were the main species. Optical adsorption investigation shows that nanostructures TiO_2 has an indirect band gap structure with an optical band gap of 3.00, 3.05 and 3.15 eV for calcination temperature at 400, 500 and 600 °C, respectively. As the calcination temperature decreases, the specific surface area increases and the photocatalyst will result in a high degradation rate of dyes. Formation of $OH^•$ free radicals during irradiation is determined by photoluminescence studies using terephtalic acid as probe molecule. The degradation extent was checked by UV–Vis. spectroscopy and confirmed by chemical oxygen demand.

References

[1] A. El Nemr, Impact, Monitoring and Management of Environmental Pollution, first ed., Nova Science Publishers, USA, 2010.
[2] A. El Nemr, Non-Conventional Textile Wastewater Treatment, first ed., Nova Science Publishers, USA, 2012.
[3] A. Houas, Photocatalytic degradation pathway of methylene blue in water, Appl. Catal. B Environ. 31 (2001) 145–157.
[4] S. Ruan, F. Wu, T. Zhang, W. Gao, B. Xu, M. Zhao, Photodegradation of dyes by a novel TiO_2/u-RuO_2/GNS nanocatalyst derived from Ru/GNS after its use as a catalyst in the aerial oxidation of primary alcohols (GNS = graphene nanosheets), Mater. Chem. Phys. 69 (2001) 7–9.
[5] S. Al-Qaradawi, S.R. Salman, Photocatalytic degradation of methyl orange as a model compound, J. Photochem. Photobiol. A Chem. 148 (2002) 161–168.
[6] B.-Y. Jia, L.-Y. Duan, C.-L. Ma, C.-M. Wang, Characterization of TiO_2 loaded on activated carbon fibers and its photocatalytic reactivity, Chin. J. Chem. 25 (2007) 553–557.
[7] M. Asilturk, F. Sayilkan, S. Erdemoglu, M. Akarsu, H. Sayilkan, M. Erdemoglu, Characterization of the hydrothermally synthesized nano-TiO_2 crystallite and the photocatalytic degradation of Rhodamine B, J. Hazard Mater. 129 (2006) 164–170.
[8] P. Wilhelm, D. Stephan, Photodegradation of rhodamine B in aqueous solution via SiO_2@TiO_2 nano-spheres, J. Photochem. Photobiol. A Chem. 185 (2007) 19–25.
[9] D.S. Kim, Y.S. Park, Photocatalytic decolorization of rhodamine B by immobilized TiO_2 onto silicone sealant, Chem. Eng. J. 116 (2006) 133–137.
[10] Y. Li, S. Sun, M. Ma, Y. Ouyang, W. Yan, Kinetic study and model of the photocatalytic degradation of rhodamine B (RhB) by a TiO_2-coated activated carbon catalyst: effects of initial RhB content, light intensity and TiO_2 content in the catalyst, Chem. Eng. J. 142 (2008) 147–155.
[11] S. Tunç, T. Gürkan, O. Duman, On-line spectrophotometric method for the determination of optimum operation parameters on the decolorization of Acid Red 66 and Direct Blue 71 from aqueous solution by Fenton process, Chem. Eng. J. 181–182 (2012) 431–442.
[12] J. Huang, H. Song, C. Chen, Y. Yang, N. Xu, X. Ji, Facile synthesis of N-doped TiO_2 nanoparticles caged in MIL100(Fe) for photocatalytic degradation of organic dyes under visible light irradiation, J. Environ. Chem. Eng. 5 (2017) 2579–2585.
[13] K. Alamelu, V. Raja, L. Shiamala, B.M. Jaffar Ali, Biphasic TiO_2 nanoparticles decorated graphene nanosheets for visible light driven photocatalytic degradation of organic dyes, Appl. Surf. Sci. 430 (2018) 145–154.
[14] S. Natarajan, H.C. Bajaj, R.J. Tayade, Recent advances based on the synergetic effect of adsorption for removal of dyes from wastewater using photocatalytic process, J. Environ. Sci. 65 (2018) 201–222.
[15] A. Hassani, L. Alidokht, A.R. Khataee, S. Karaca, Optimization of comparative removal of two structurally different basic dyes using coal as a low-cost and available adsorbent, J. Taiwan Inst. Chem. Eng. 45 (2014) 1597–1607.
[16] E. Ayranci, O. Duman, In-situ UV-visible spectroscopic study on the adsorption of some dyes onto activated carbon cloth, Separ. Sci. Technol. 44 (2009) 3735–3752.
[17] O. Duman, S. Tunç, T.G. Polat, Adsorptive removal of triarylmethane dye (Basic Red 9) from aqueous solution by sepiolite as effective and low-cost adsorbent, Microporous Mesoporous Mater. 210 (2015) 176–184.
[18] O. Duman, S. Tunç, T.G. Polat, Determination of adsorptive properties of expanded vermiculite for the removal of C.I. Basic Red 9 from aqueous solution: kinetic, isotherm and thermodynamic studies, Appl. Clay Sci. 109–110 (2015) 22–32.
[19] O. Duman, S. Tunç, T.G. Polat, B.K. Bozoğlan, Synthesis of magnetic oxidized multiwalled carbon nanotube-κ-carrageenan-Fe_3O_4 nanocomposite adsorbent and its application in cationic Methylene Blue dye adsorption, Carbohydr. Polym. 147 (2016) 79–88.
[20] O. Duman, S. Tunç, B.K. Bozoğlan, T.G. Polat, Removal of triphenylmethane and reactive azo dyes from aqueous solution by magnetic carbon nanotube-κ-carrageenan-Fe_3O_4 nanocomposite, J. Alloy. Comp. 687 (2016) 370–383.
[21] X. Wang, X. Cheng, X. Yu, X. Quan, Study on surface enhanced Raman scattering substrate based on titanium oxide nanorods coated with gold nanoparticles, J. Nanotechnol. (2018). Hindawi publishing.
[22] W. Chakhari, J. Ben Naceur, S. Ben Taieb, I. Ben Assaker, R. Chtourou, Fe-doped TiO_2 nanorods with enhanced electrochemical properties as efficient photoanode materials, J. Alloy. Comp. 708 (2017) 862–870.
[23] T. Azis, A.T. Nurwahidah, D. Wibowo, M. Nurdin, Photoelectrocatalyst of Fe codoped N-TiO_2/Ti nanotubes: pesticide degradation of thiamethoxam under UV–visible lights, Environ. Nanotechnol. Monit. Managem. 8 (2017) 103–111.
[24] Q. Wang, R. Jin, M. Zhang, S. Gao, Solvothermal preparation of Fe-doped TiO_2 nanotube arrays for enhancement in visible light induced photoelectrochemical performance, J. Alloy. Comp. 690 (2017) 139–144.
[25] C.W. Soo, J.C. Juan, C.W. Lai, S.B.A. Hamid, R.M. Yusop, Fe-doped mesoporous anatase-brookitetitania in the solar-light-induced photodegradation of Reactive Black 5 dye, J. Taiwan Inst. Chem. Eng. 68 (2016) 153–161.
[26] S. Larumbe, M. Monge, C. G′omez-Polo, Comparative study of (N, Fe) doped TiO_2 photocatalysts, Appl. Surf. Sci. 327 (2015) 490–497.
[27] R. Shirley, The CRYSFIRE System for Automatic Powder Indexing: User's Manual, 41 Guildford, The Lattice Press, Park Avenue, Guildford, Surrey GU2 7NL, England, 2002.
[28] A.A. El-Bindary, S.M. El-Marsafy, A.A. El-Maddah, Enhancement of the photocatalytic activity of ZnO nanoparticles by silver doping for the degradation of AY99 contaminants, J. Mol. Struct. 1191 (2019) 76–84.
[29] H.A. Kiwaan, T.M. Atwee, E.A. Azab, A.A. El-Bindary, Efficient photocatalytic degradation of acid red 57 using synthesized ZnO nanowires, J. Chin. Chem. Soc. 66 (2019) 89–98.
[30] H.B. Hadjltaief, M.B. Zina, M.E. Galvez, P.D. Costa, Photocatalytic degradation of methyl green dye in aqueous solution over natural clay-supported ZnO-TiO_2 catalysts, J. Photochem. Photobiol. A Chem. 315 (2016) 25–33.
[31] M. Alijani, B.K. Kaleji, Optical and structural properties of TiO2 nanopowders with Ce/Sn doping at various calcination temperature and time, Opt. Quant. Electron. 49 (2017) 34–49.
[32] S. Brunauer, P.H. Emmett, E. Teller, Adsorption of gases in multimolecular layers, J. Am. Chem. Soc. 60 (1938) 309–319.
[33] Q. Zhang, M. Xu, B. You, Q. Zhang, H. Yuan, K. Ostrikov, Oxygen vacancy-mediated ZnO nanoparticle photocatalyst for degradation of methylene blue, Appl. Sci. 8 (2018) 353–364.
[34] Y.-C. lee, Y.S. Chang, L.G. Teoh, Y.L. Huang, Y.C. Shen, The effects of the nanostructure of mesoporous TiO_2 on optical band gap energy, J. Sol. Gel Sci. Technol. 56 (2010) 33–38, 9.
[35] K. Fischer, P. Schulz, I. Atanasov, A. Abdul Latif, I. Thomas, M. Kühnert, A. Prager, J. Griebel, A. Schulze, Synthesis of high crystalline TiO_2 nanoparticles on a polymer membrane to degrade pollutants from water, Catalysts 8 (2018) 376–391.
[36] B. Jin, X.S. Zhou, J. Luo, X. Xu, L. Ma, D. Huang, Z. Shao, Z. Luo, Fabrication and characterization of high efficiency and stable Ag_3PO_4/TiO_2 nanowire array heterostructure photoelectrodes for the degradation of methyl orange under visible light irradiation, RSC Adv. 5 (2015) 48118–48123.
[37] A.L. Patterson, The Scherrer formula for X-Ray particle size determination, Phys. Rev. 56 (1939) 978–982.
[38] M. Mirzaei, S. Sabbaghi, M.M. Zerafat, Photo-catalytic degradation of formaldehyde using nitrogen-doped TiO_2 nano-photocatalyst: statistical design with response surface methodology (RSM), Canad. J. Chem. Eng. 96 (2018) 2544–2552.
[39] H. Narayan, H. Alemu, A Comparison of photocatalytic activity of TiO_2

nanocomposites doped with Zn^{2+}/Fe^{3+} and Y^{3+} ions, Int. J. Nanosci. Nanotechnol. 13 (2017) 315–325.
[40] A. Jain, D. Vaya, Photocatalytic activity of TiO_2 nanomaterial, J. Chil. Chem. Soc. 62 (2017) 3683–3690.
[41] J. Tauc, R. Grigorovici, A. Vancu, Optical properties and electronic structure of amorphous germanium, Phys. Status Solidi B 15 (1966) 627–637.
[42] P. Wang, S. Zhan, Y. Xia, S. Ma, Q. Zhou, Y. Li, The fundamental role and mechanism of reduced graphene oxide in rGO/Pt-TiO_2 nanocomposite for high-performance photocatalytic water splitting, Appl. Catal. B Environ. 207 (2017) 335–346.
[43] X. Zheng, W. Fu, F. Kang, H. Peng, J. Wen, Enhanced photo-Fenton degradation of tetracycline using TiO_2-coated α-Fe_2O_3 core–shell heterojunction, J. Ind. Eng. Chem. 68 (2018) 14–23.
[44] J.I. Pankove, Optical Process in Semiconductors, Prentice- Hall, New Jersey, 1971.
[45] D. Yoo, I. Kim, S. Kim, C.H. Hahn, C. Lee, S. Cho, Effects of annealing temperature and method on structural and optical properties of TiO_2 films prepared by RF magnetron sputtering at room temperature, Appl. Surf. Sci. 253 (2007) 3888–3892.
[46] T. Sun, J. Fan, E.Z. Liu, L.S. Liu, Y. Wang, H.Z. Daia, Y.H. Yang, W.Q. Hou, X.Y. Hu, Z.Y. Jiang, Fe and Ni co-doped TiO_2 nanoparticles prepared by alcohol-thermal method: application in hydrogen evolution by water splitting under visible light irradiation, Powder Technol. 228 (2012) 210–218.
[47] G. Li, B.-D. Wang, Q. Sun, W.-Q. Xu, Y.-F. Han, Visible-Light photocatalytic activity of Fe and/or Ni doped ilmenite derived-titanium dioxide nanoparticles, J. Nanosci. Nanotechnol. 19 (2019) 3343–3355.
[48] X. Sun, L. Yan, R. Xu, M. Xu, Y. Zhu, Surface modification of TiO_2 with polydopamine and its effect on photocatalytic degradation mechanism, Colloids Surf., A (2019). https://doi.org/10.1016/j.colsurfa.2019.03.018.
[49] K.Z. Elwakeel, A.A. El-Bindary, E.Y. Kouta, E. Guibal, Functionalization of polyacrylonitrile/Na-Y-zeolite composite with amidoxime groups for the sorption of Cu(II), Cd(II) and Pb(II) metal ions, Chem. Eng. J. 332 (2018) 727–736.
[50] K.M. Reza, A. Kurny, F. Gulshan, Parameters affecting the photocatalytic degradation of dyes using TiO_2: a review, Appl. Water Sci. 7 (2018) 1569–1578.
[51] M.M. Haque, M. Muneer, TiO_2-mediated photocatalytic degradation of a textile dye derivative, bromothymol blue, in aqueous suspensions, Dyes Pigments 75 (2007) 443–448.
[52] R.S. Dariani, A. Esmaeili, A. Mortezaali, S. Dehghanpour, Photocatalytic reaction and degradation of methylene blue on TiO_2 nano-sized particles, Optik 127 (2016) 7143–7154.
[53] D.M. El-Mekkawi, H.R. Galal, R.M. Abd El Wahab, W.A.A. Mohamed, Photocatalytic activity evaluation of TiO_2 nanoparticles based on COD analyses for water treatment applications: a standardization attempt, Int. J. Environ. Sci. Technol. 13 (2016) 1077–1088.
[54] A. Olad, S. Behboud, A.A. Entezami, Preparation, characterization and photocatalytic activity of TiO_2/polyaniline core-shell nanocomposite, Bull. Mater. Sci. 35 (2012) 801–809.
[55] R.S. Sabry, Y.K. Al-Haidarie, M.A. Kudhier, Synthesis and photocatalytic activity of TiO_2 nanoparticles prepared by sol–gel method, J. Sol. Gel Sci. Technol. 78 (2016) 299–306.
[56] M. Anas, D.S. Han, K. Mahmoud, H. Park, A. Abdel-Wahab, Photocatalytic degradation of organic dye using titanium dioxide modified with metal and non-metal deposition, Mater. Sci. Semicond. Process. 41 (2016) 209–218.
[57] C. Hou, B. Hu, J. Zhu, Photocatalytic degradation of methylene blue over TiO_2 pretreated with varying concentrations of NaOH, Catalysts 8 (2018) 575–587.
[58] E. Adamek, J. Ziemianska, I. Lipska, A. Makowski, A. Sobczak, W. Baran, Assessment of radiant flux absorption by irradiated phase on the kinetics of photocatalytic reactions, Physicochem. Probl. Miner. Process. 45 (2010) 5–14.
[59] R. Singh, S. Dutta, Synthesis and characterization of solar photoactive TiO_2 nanoparticles with enhanced structural and optical properties, Adv. Powder Technol. 29 (2018) 211–219.
[60] F. Huang, L. Chen, H. Wang, Z. Yan, Analysis of the degradation mechanism of methylene blue by atmospheric pressure dielectric barrier discharge plasma, Chem. Eng. J. 162 (2010) 250–256.
[61] A.R. Khataee, M.B. Kasiri, Photocatalytic degradation of organic dyes in the presence of nanostructured titanium dioxide: influence of the chemical structure of dyes, J. Mol. Catal. A Chem. 328 (2010) 8–26.
[62] B.A. van Driel, P.J. Kooyman, K.J. van den Berg, A. Schmidt-Ott, J. Dik, A quick assessment of the photocatalytic activity of TiO_2 pigments-From lab to conservation studio, Micro J. 126 (2016) 162–171.
[63] Y. Nam, J.H. Lim, K.C. Ko, J.Y. Lee, Photocatalytic activity of TiO_2 nanoparticles: a theoretical aspect, J. Mater. Chem. 7 (2019) 13833–13859.
[64] A. Ajmal, I. Majeed, R.N. Malik, H. Idriss, M.A. Nadeem, Principles and mechanisms of photocatalytic dye degradation on TiO_2 based photocatalysts: a comparative overview, RSC Adv. 4 (2014) 37003–37026.
[65] X.H. Lin, S.N. Lee, W. Zhang, S.F.Y. Li, Photocatalytic degradation of terephthalic acid on sulfated titania particles and identification of fluorescent intermediates, J. Hazard Mater. 303 (2016) 64–75.
[66] G. Crini, Kinetic and Equilibrium studies on the removal of cationic dyes from aqueous solution by adsorption onto a cyclodextrin polymer, Dyes Pigments 77 (2008) 415–426.
[67] A.A. El-Bindary, H.A. Kiwaan, A.F. Shoair, A.R. hawas, A novel crosslinked amphoteric adsorbent thiourea formaldehyde calcium alginate: preparation, characterization and adsorption behaviors of removing color from acidic and basic dyes, Desalin. Water Treat. 151 (2019) 145–160.